Electric Drive Based on an Open-End Winding Surface PM Synchronous Machine With a Floating Capacitor Bridge

Albino Amerise, Luca Rovere , *Member, IEEE*, Andrea Formentini , *Member, IEEE*, Michele Mengoni , *Member, IEEE*, Luca Zarri , *Senior Member, IEEE*, and Pericle Zanchetta , *Fellow, IEEE*

Abstract—A speed control scheme is presented for a three-phase surface permanent magnet synchronous machine with an open-end stator winding fed by a three-phase inverter and a floating bridge inverter. The latter is used to compensate for the reactive power of the main inverter and to maximize the active power received by the motor, without exceeding the available stator current and dc-link voltage. To reduce the switching losses, the dc-link voltage of the floating inverter bridge varies depending on the operating condition of the motor and the controllability requirements of the system. The experimental results show that a significant improvement in the speed range at constant power is achievable, proportionally to the dc-link voltage of the floating bridge inverter.

Index Terms—AC motors, motor drives, multilevel systems, permanent magnet machines, pulse-width modulated (PWM) inverters, variable speed drives.

I. INTRODUCTION

A HIGH torque density makes surface permanent magnet synchronous machines (SPMSMs) suitable for industrial applications if they are not required to operate over a wide speed range. Interior permanent magnet synchronous machines, which use ferrite magnets and compensate the resulting reduction in the flux level with the reluctance torque due to the rotor anisotropy, are preferred in spindle-drive applications.

Albino Amerise, Michele Mengoni, and Luca Zarri are with the Department of Electrical, Electronic and Information Engineering "G. Marconi", University of Bologna, Bologna 40136, Italy (e-mail: albino.amerise2@unibo.it; michele.mengoni@unibo.it; luca.zarri2@unibo.it).

Luca Rovere and Andrea Formentini are with the Department of Electrical and Electronic Engineering, The University of Nottingham, Nottingham NG7 2RD, U.K. (e-mail: luca.rovere@nottingham.ac.uk; andrea.formentini@nottingham.ac.uk).

Pericle Zanchetta is with the Department of Electrical and Electronic Engineering, The University of Nottingham, Nottingham NG7 2RD, U.K., and also with the Department of Electrical, Computer and Biomedical Engineering, University of Pavia, Pavia 27100, Italy (e-mail: pericle.zanchetta@nottingham.ac.uk).

Color versions of one or more of the figures in this article are available online at http://ieeexplore.ieee.org.
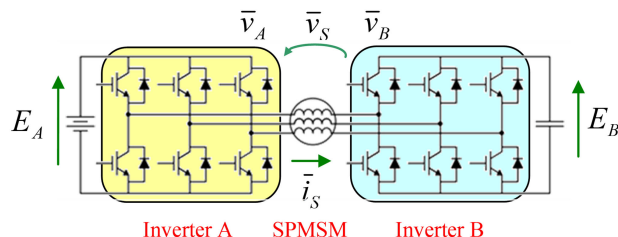
Fig. 1. Electric drive with a floating capacitor bridge and an open-end winding machine.

Nevertheless, the use of a solid rotor core in SPMSMs has several advantages, such as simplifying the manufacturing process, better robustness and efficiency, and lower costs, so several solutions to widen the motor speed range have been developed and can be found in the literature. The simplest one is the use of a step-up converter to boost the dc-link of the main inverter. However, this topology requires adding some bulk inductors at the input of the converter, and the boost ratio is generally not higher than two [1]. Other solutions include the use of two inverters to feed a motor with open-end windings [2]. Two separated voltage sources can supply both sides of the stator winding and increase the phase voltage. If two separated power sources are not available, the inverters can share the same dc-link [3]. However, this solution causes the problem of the common-mode current, which can circulate in the drive. A modulation strategy for this dual inverter was investigated in [4], where two different technologies (Si and SiC) were adopted for the switches of the main inverter and the floating bridge, depending on the respective switching frequencies. The problem of the zero-sequence current was thoughtfully discussed in [5], [6].

Finally, another dual inverter topology that is capable of improving the performance of SPMSMs is the one represented in Fig. 1, where the second inverter is a floating capacitor bridge [7], [8]. The drive presented in this article is based on this topology.

The dual inverter with a floating capacitor bridge not only extends the motor speed range but can supply the machine with a multilevel pulse-width modulated (PWM) voltage to reduce the current ripple, which can be quite significant for PM machines with a low number of turns and a small synchronous inductance [9], [10]. The floating inverter bridge can be used as a power factor compensator of the main inverter, which can transfer the

maximum active power to the motor over the whole speed range. The same topology has also been developed for induction motors [11], [12].

The control scheme of this configuration was analyzed in [13]–[15]. In particular, the work [13] starts from the observation that a series inductance can significantly change the constant power speed range of a PM brushless machine, but it reduces the base speed. Conversely, a floating capacitor bridge can be controlled to operate as a variable inductance when needed. The floating capacitor reference is initially set to zero. To reduce the switching losses of the compensation inverter, the floating-capacitor-voltage reference is raised to its nominal value only when the motor current exceeds a threshold value. Basically, a current-oriented reference frame is used to control the floating capacitor converter, and the performance of the drive is assessed for different inverter ratings.

Finally, some techniques to estimate the machine parameters were discussed in [16].

The main contribution of this article is to improve the results obtained in [13]–[15] and illustrate a field-oriented control scheme that can fully exploit the torque and power capability of an SPMSM with open-end windings. The analysis is performed as a constrained optimization problem, where the machine thermal current and the voltage ratings of the inverters limit the torque capability. Also, to reduce the switching losses, the dc-link voltage of the floating capacitor bridge is adjusted depending on the operating condition of the motor. The motor state corresponding to the maximum torque is identified through a theoretical analysis of the operating conditions.

II. SYSTEM MODEL

A. Machine and Floating Bridge Capacitor Equations

With reference to Fig. 1, the voltage applied to the three-phase stator winding can be expressed as follows:

$$\bar{v}_S = \bar{v}_A - \bar{v}_B \tag{1}$$

where $\bar{v}_S$, $\bar{v}_A$, and $\bar{v}_B$ are the voltage space vectors of the motor, inverter A, and inverter B, respectively.

The mathematical model of an SPMSM can be written in a d–q reference frame with the d-axis aligned with the excitation flux as follows:

$$v_{Sd} = R_S i_{Sd} - \omega \varphi_{Sq} + \frac{d\varphi_{Sd}}{dt} \tag{2}$$

$$v_{Sq} = R_S i_{Sq} + \omega \varphi_{Sd} + \frac{d\varphi_{Sq}}{dt} \tag{3}$$

$$\varphi_{Sd} = L_S i_{Sd} + \varphi_e \tag{4}$$

$$\varphi_{Sq} = L_S i_{Sq} \tag{5}$$

$$T = \frac{3}{2} p \varphi_e i_{Sq} \tag{6}$$

where ω is the angular frequency of the rotor speed in electric radians, p is the number of pole pairs, T is the electromagnetic torque, i_{Sd} and i_{Sq} are the d–q components of the stator current vector $\bar{i}_S$, φ_{Sd} and φ_{Sq} are the d–q components of the stator flux

vector $\bar{\varphi}_S$, φ_e is the excitation flux, L_S and R_S are the stator inductance and resistance, respectively.

The voltage across the floating capacitor C is related to its electrostatic energy, which varies at the following rate:

$$\frac{d}{dt}\left(\frac{1}{2}CE_B^2\right) = \frac{3}{2}\bar{i}_S \cdot \bar{v}_B \tag{7}$$

where E_B is the dc-link voltage of inverter B and "·" is the dot product, calculated by summing the products of the corresponding d and q components of the first and second vector.

B. Control Strategy

The control scheme for the floating capacitor is implemented in a rotating reference frame that is synchronous with the stator current space vector $\bar{i}_S$. The output voltage of the floating bridge can be expressed as follows:

$$\bar{v}_B = (v_B^p + jv_B^q)\frac{\bar{i}_S}{|\bar{i}_S|} \tag{8}$$

where v_B^p and v_B^q are respectively the parallel and orthogonal components of $\bar{v}_B$ to $\bar{i}_S$, which are proportional to the active and reactive power of inverter B.

In this reference frame, (7) becomes

$$\frac{d}{dt}\left(\frac{1}{2}CE_B^2\right) = \frac{3}{2}|\bar{i}_S|\,v_B^p \tag{9}$$

which shows that it is possible to control the derivative of the energy in the floating bridge and, consequently, its voltage by acting on the parallel component of $\bar{v}_B$.

Therefore, v_B^p is zero at steady state, while the orthogonal component v_B^q is a degree of freedom that can be used to control the reactive power of the floating bridge inverter.

The active power P_A of inverter A must be consistent with the voltage and current capability of the power source. The value of P_A is linked to the reactive power Q_A through the following expression:

$$P_A^2 + Q_A^2 = \left(\frac{3}{2}|\bar{i}_S|\,|\bar{v}_A|\right)^2. \tag{10}$$

At steady state, active power P_A includes the Joule losses, the iron losses, and the mechanical power delivered to the motor (the active power transferred to inverter B is negligible), while the right-hand side of (10) represents the square of the apparent power of inverter A.

The reactive power Q_A can be written as follows:

$$Q_A = \frac{3}{2}\bar{v}_A \cdot j\bar{i}_B = Q_S + Q_B \tag{11}$$

where Q_S and Q_B are respectively the reactive power of the SPMSM and inverter B.

Equation (11) shows that it is possible to nullify the reactive power of inverter A if the reactive power of inverter B is equal to $-Q_S$, and therefore to maximize the transferable active power in compliance with (10), given the values of $|\bar{v}_A|$ and $|\bar{i}_S|$.

By combining (2), (3), and (11) at steady state, and by neglecting the voltage drop due to the stator resistance, Q_A can be

expressed as follows:

$$Q_A \cong \frac{3}{2} \left(j\omega\bar{\varphi}_S \right) \cdot j\bar{i}_S + \frac{3}{2} \bar{v}_B \cdot j\bar{i}_S. \tag{12}$$

Equating (12) to zero and considering (8) leads to the expression of the orthogonal component v_B^q

$$v_{B,\mathrm{opt}}^q = -\frac{\omega\bar{\varphi}_S \cdot \bar{i}_S}{|\bar{i}_S|}. \tag{13}$$

Combining (8), (9), and (13) allows finding the expression of $\bar{v}_B$ as a function of the rotor speed ω and of the motor state

$$\bar{v}_B = \left[\frac{d}{dt} \left(\frac{1}{3} C E_B^2 \right) - j\frac{\omega\bar{\varphi}_S \cdot \bar{i}_S}{|\bar{i}_S|} \right] \frac{\bar{i}_S}{|\bar{i}_S|}. \tag{14}$$

Equation (14) shows that $\bar{v}_B$ is orthogonal to the stator current at steady state. This equation is independent of the type of machine and has been found also for induction motors [12].

C. Current and Voltage Constraints

The torque characteristic is limited by the voltage and current capability of the inverter and the SPMSM. At low speed, the behavior of the machine is affected by the value of the admissible stator current $I_{\max}$, which can be the nominal thermal current of the machine at steady state or the nominal current of the inverters in transient overload conditions. In SPMSMs with NeFeB magnets and not operating in overload conditions, $I_{\max}$ is usually lower than φ_e/L_S because the thickness of the airgap does not allow the stator inductance to reach values high enough.

Furthermore, above the base speed, the machine behavior is constrained by the available dc-link voltage of inverters A and B. These constraints can be expressed as follows:

$$|\bar{v}_A| \leq V_{A,\max} \tag{15}$$

$$|\bar{v}_B| \leq V_{B,\max} \tag{16}$$

where $V_{A,\max}$ and $V_{B,\max}$ depend on the available dc voltage of inverters A and B, and on the modulation strategy. If space-vector PWM is used, the maximum voltages generated by the two inverters in the linear range of modulation are as follows:

$$V_{A,\max} = \frac{E_A}{\sqrt{3}} \tag{17}$$

$$V_{B,\max} = \frac{E_B}{\sqrt{3}}. \tag{18}$$

Inequality (16) for inverter B, combined with (14), can be rewritten at steady state as a function of the components i_{Sd} and i_{Sq} of the stator current vector by means of (4) and (5)

$$\left| L_S |\bar{i}_S| + \varphi_e \frac{i_{Sd}}{|\bar{i}_S|} \right| \leq \frac{V_{B,\max}}{|\omega|}. \tag{19}$$

Similarly, in steady-state operating conditions, if the voltage drop due to the stator resistance is neglected, (8), combined with (1)–(5) and (14), leads to the following inequality for inverter A:

$$\varphi_e \left| \frac{i_{Sq}}{\bar{i}_S} \right| \leq \frac{V_{A,\max}}{|\omega|}. \tag{20}$$

Inequalities (19) and (20) are valid only if $\bar{v}_B$ is given by (14). In steady-state conditions, if the rotor speed ω is so that v_B^q given by (13) violates (16), the expression for $\bar{v}_B$ becomes the following:

$$\bar{v}_B = j \left(\mathrm{sgn}\, v_{B,\mathrm{opt}}^q \right) V_{B,\max} \frac{\bar{i}_S}{|\bar{i}_S|}. \tag{21}$$

By substituting (21) in (12) and considering (13) and (19), the reactive power Q_A turns out to be different from zero

$$Q_A = \frac{3}{2} \left[\omega \left(L_S |\bar{i}_S|^2 + \varphi_e i_{Sd} \right) + \left(\mathrm{sgn}\, v_{B,\mathrm{opt}}^q \right) V_{B,\max} |\bar{i}_S| \right] \tag{22}$$

and (20) must be replaced by the following inequality:

$$\left| \left(L_S + \frac{\left(\mathrm{sgn}\, v_{B,\mathrm{opt}}^q \right) V_{B,\max}}{|\omega| |\bar{i}_S|} \right) \bar{i}_S + \varphi_e \right| \leq \frac{V_{A,\max}}{|\omega|}. \tag{23}$$

The admissible domain of the stator current vector resulting from the voltage and current capability of the drive can be plotted in a complex plane, where the horizontal and vertical axes are respectively i_{Sd} and i_{Sq}, as shown in Fig. 2.

The current vectors satisfying the constraint on the stator current are those delimited by a circle with constant radius $I_{\max}$. The curves coming from the voltage constraints (19) and (20), which tend to reduce as ω increases and depend on the values of the system parameters, establish the domain of the current vectors that can be injected into the machine at a given speed. The area defined by (15) corresponds to a pair of vertical angles (with a blue border), while the area defined by (16) has a cardioid-like shape (with a green border). It is worth noting that these curves are very different from those of a traditional SPM motor drive and have a non-null intersection, highlighted in green, even at high speed.

At a given speed, (6) says that the highest torque is generated if the stator current i_{Sq} reaches a maximum in the admissible domain represented by a dashed area in Fig. 2. Therefore, the analysis of the loci of Fig. 2 is essential for the calculation of the torque capability of the drive.

D. Resulting Speed Ranges

The base speed ω_{base} of a dual inverter system can be calculated by (20) with i_{Sq} equal to $I_{\max}$ and i_{Sd} equal to zero

$$\omega_{\mathrm{base}} = \frac{V_{A,\max}}{\varphi_e}. \tag{24}$$

For a comparison, the base speed ω'_{base} of an SPMSM fed by a single inverter can be approximately found under the assumption that the electrical input power is totally converted into mechanical power

$$\omega'_{\mathrm{base}} T = \frac{3}{2} V_{A,\max} I_{A,\max} \cos\Phi_{\mathrm{base}} \tag{25}$$

where Φ_{base} is the phase angle between $\bar{v}_A$ and $\bar{i}_S$ at the base speed. If i_{Sq} is equal to $I_{\max}$, the magnitude of $\bar{v}_A$ is $V_{A,\max}$, combining (6), (24), and (25), it turns out that

$$\omega'_{\mathrm{base}} = \omega_{\mathrm{base}} \cos\Phi_{\mathrm{base}}. \tag{26}$$
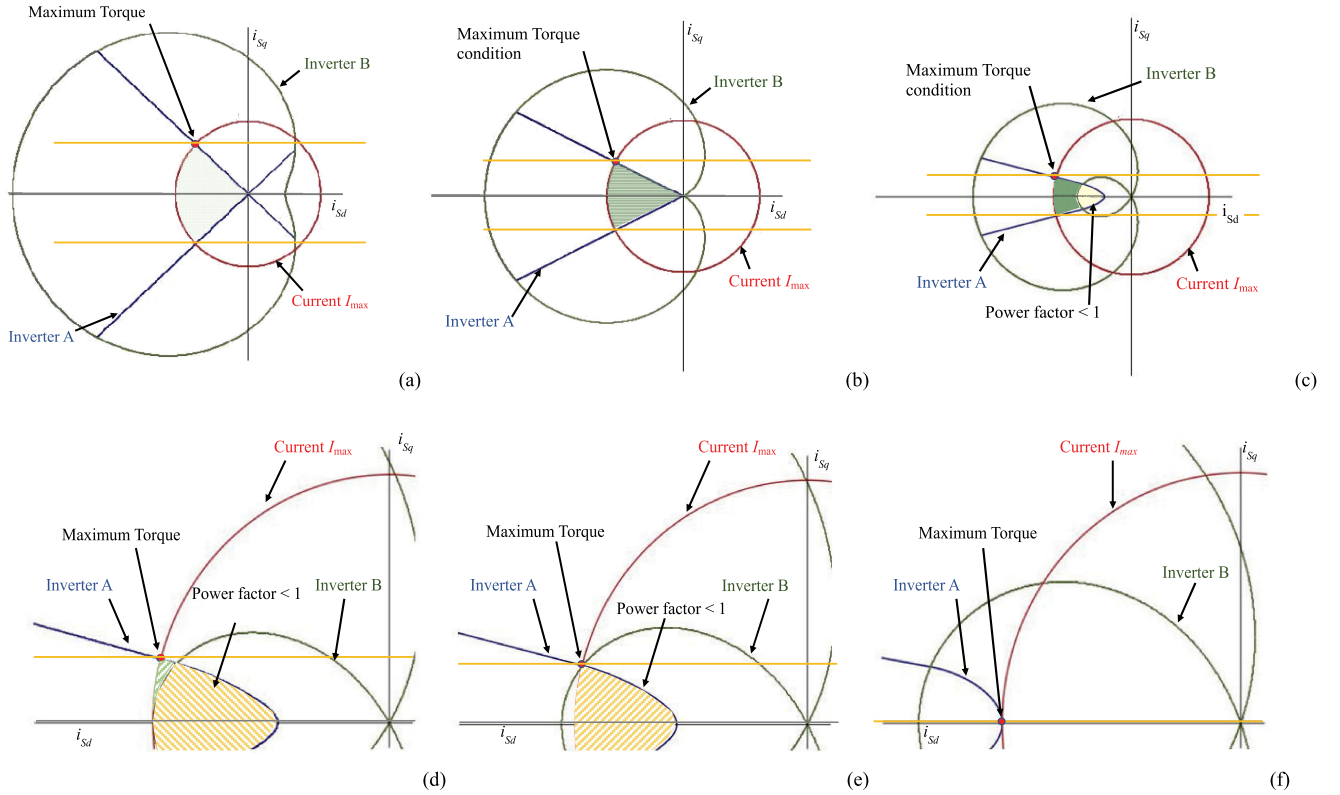
Fig. 2. Representation of the voltage and current constraints in plane i_{Sd}–i_{Sq} for a dual inverter drive. Curves (a), (b), and (c) are plotted at increasing values of ω greater than ω_{base} and lower that ω_{PF}. Curves (d), (e), and (f) are plotted respectively at $\omega = \omega_{\text{PF}}$, $\omega = \omega_{\text{pow}}$ (e) and $\omega = \omega_{\text{max}}$ (f).

Consequently, the base speed of a single inverter drive is lower than that of a dual inverter drive and proportional to the input power factor at the base speed.

Above the base speed up to a threshold value, the domain obtained by intersecting the areas delimited by the three curves of Fig. 2 is a circular sector, as shown in Fig. 2(a) and (b). However, at higher speeds, the admissible operating domain can be split into two parts, as shown in Fig. 2(c). The first one (in green) is composed of operating states with unity power factor. The second one (in yellow) is characterized by operating states with a power factor lower than one because the domain of (16) is disconnected, and (19) is replaced by (21). For any value of torque between the yellow lines, there always exists an operating state with unity power factor. If the speed increases further, it is not possible to meet this condition anymore because the domain with a power factor lower than one becomes predominant. Fig. 2(d) is drawn at speed ω_{PF}, when the curve of the voltage constraint of inverter B becomes tangent to the circle of the maximum current. Starting from this speed, low values of torque cannot be generated at unity power factor. The value of ω_{PF} can be found from (19) with i_{Sd} equal to $-I_{\text{max}}$

$$\omega_{\text{PF}} = \frac{V_{B,\text{max}}}{\varphi_e - L_S I_{\text{max}}}. \tag{27}$$

Above ω_{PF}, intersecting (19), considered as an equality, with the current constraint allows calculating the minimum torque

that can be generated at unity power factor

$$T_{\text{PF}} = \frac{3}{2} p \varphi_e I_{\text{max}} \sqrt{1 - \left(k + \frac{\omega_{\text{base}}}{\omega} r\right)^2} \tag{28}$$

where

$$k = \frac{L_S I_{\text{max}}}{\varphi_e} \tag{29}$$

$$r = \frac{V_{B,\text{max}}}{V_{A,\text{max}}}. \tag{30}$$

It can be noted that T_{PF} is proportional to the maximum torque by a factor that is a function of the key parameters of the electric drive.

Fig. 2(e) is drawn at speed ω_{pow}, at which the admissible operating domain does not include any state with unity power factor. This value of the rotor speed is the upper bound of the constant power speed range. By intersecting (19), (20), and the current constraint, its analytical expression of ω_{pow} can be written as follows:

$$\omega_{\text{pow}} = \omega_{\text{base}} \frac{1 + r^2}{-r\,k + \sqrt{1 + r^2 - k^2}}. \tag{31}$$

The motor can reach higher speeds than ω_{pow}, but the power factor is lower than one for any torque. The maximum speed is reached when the torque, hence the mechanical power, becomes zero, as shown in Fig. 2(f). In this condition, both inverters generate only reactive power. Considering (22) and neglecting
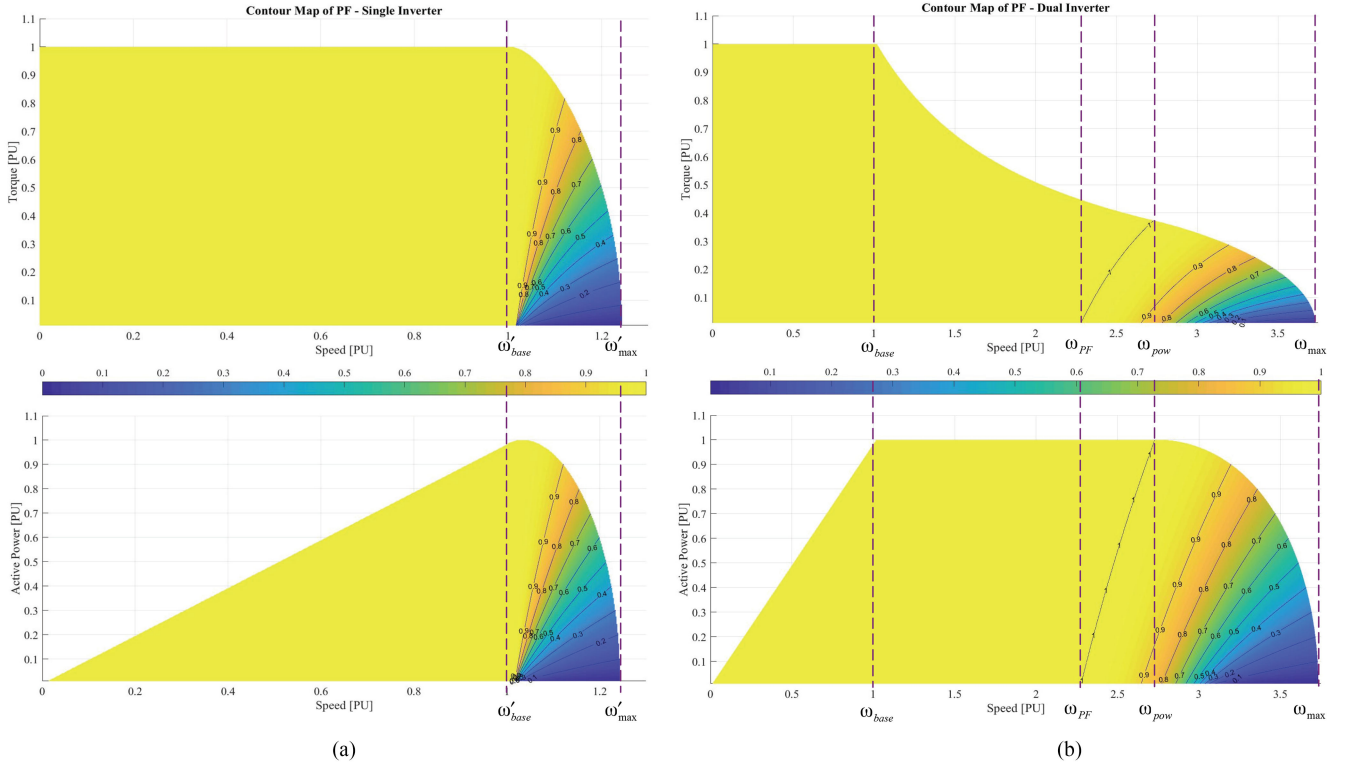
Fig. 3. Performance of the drive over the speed range normalized by the base speed of the single inverter drive, in terms of torque (top), power (bottom) and power factor (colormap). Single inverter (a) and dual inverter (b) systems with $E_B = 2\,E_A$.

the Joule and iron losses, (10) can be rewritten as follows:

$$\frac{3}{2}\left|\omega\bar{\varphi}_S \cdot \bar{i}_S + \left(\text{sgn } v_{B,\text{opt}}^q\right) V_{B,\text{max}}\left|\bar{i}_S\right|\right| = \frac{3}{2}V_{A,\text{max}}I_{\text{max}}. \tag{32}$$

Substituting (3) and (4) in (32) leads to the following expression for the maximum speed of a dual inverter drive:

$$\omega_{\text{max}} = \frac{V_{A,\text{max}} + V_{B,\text{max}}}{\varphi_e - L_S I_{\text{max}}}. \tag{33}$$

Combing (1)–(4), (8) and neglecting the voltage drop on the stator resistance, it is possible to calculate the maximum speed that can be reached in the field-weakening operation by the same machine fed by a single inverter. When i_{Sq} is zero and i_{Sd} is equal to $-I_{\text{max}}$, one finds the following result:

$$\omega'_{\text{max}} = \frac{V_{A,\text{max}}}{\varphi_e - L_S I_{\text{max}}}. \tag{34}$$

Thus, the speed ratio in these two cases is equal to

$$\frac{\omega_{\text{max}}}{\omega'_{\text{max}}} = 1 + \frac{V_{B,\text{max}}}{V_{A,\text{max}}}. \tag{35}$$

If the dc-link voltage of inverter B is twice that of inverter A, the speed range of the dual inverter system is three times as wide as that of a single inverter drive. Furthermore, this asymmetric choice allows increasing the quality of the phase voltage and makes the dual inverter system equivalent to a four-level multilevel neutral point clamped (NPC) inverter in terms of generable voltage steps.

TABLE I
PARAMETERS

P_{rated}	=	0.9	kW	R_S	= 0.24	Ω
$I_{S,rated}$	=	13	A$_{\text{peak}}$	L_S	= 0.0012	H
φ_e	=	0.0852	Wb	J_{tot}	= 0.03	Kg m^2
$\omega_{m,rated}$	=	1600	rpm	p	= 3	
$E_{A,max}$	=	80	V	$E_{B,max}$	= 160	V
C	=	160	μF			

The resulting speed ranges and the power factors for the same motor fed by a single and a dual inverter are shown in Fig. 3, which have been plotted under the assumptions that the voltage drop on the stator resistance and the iron losses are negligible. The parameters adopted to draw the curves are those of a low-power prototype used to carry out the experimental results presented in Section V. The parameters are listed in Table I.

As can be seen, the dual inverter system produces a significant increase in the speed range of the drive. In a single-inverter drive, above the base speed, a considerable fraction of the stator voltage is necessary to inject a negative value of current i_{Sd} so as to reduce the back electromotive force that limits the circulation of torque-producing current i_{Sq}. Conversely, in the dual inverter system, the voltage generated by inverter B to keep the unity input power factor, helps compensate for the q-axis back electromotive force, thus extending the constant power speed range. If the speed increases up to ω_{pow}, the voltage
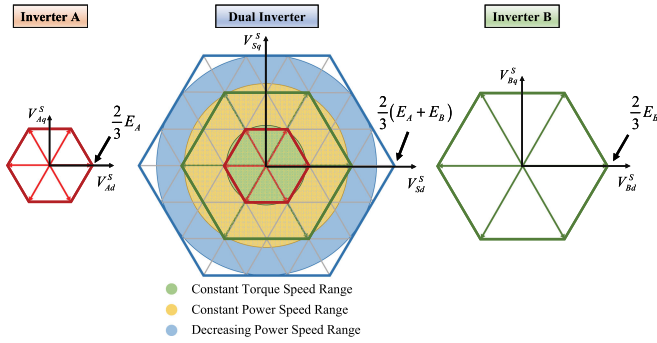
Fig. 4. Voltage vectors generated by inverter A, the dual inverter system and inverter B when E_B is $2E_A$. Superscript "S" is used to identify quantities in the stator reference frame.

required to compensate for the reactive power violates (19), and it is necessary to use the voltage of the main power source as it happens in a single-inverter system.

To clarify the exploitation of the available voltage in a dual inverter system, Fig. 4 shows the voltages that can be generated by inverter A, inverter B, and the dual system. The inner circle, in light green, represents the set of voltage $\bar{v}_S$ applied to the stator winding of the machine in the constant torque speed range. This circle slightly exceeds the voltage hexagon of inverter A because a small amount of voltage is demanded to inverter B to keep the power factor equal to one.

The mid circle area, in yellow, shows the voltage vectors used in the constant-power speed range. The radius of this area can be calculated by assuming that $\bar{v}_S$ is the vector difference of $\bar{v}_A$ and $\bar{v}_B$, respectively, with magnitudes equal to $V_{A,\max}$ and $V_{B,\max}$ and orthogonal to one another.

If it is necessary to increase $\bar{v}_S$ further, the voltage vectors $\bar{v}_A$ and $\bar{v}_B$ cannot be orthogonal anymore and tend to the operating condition where they are opposite to each other. The voltage applied to the stator winding reaches its maximum amplitude given by $V_{A,\max} + V_{B,\max}$ in the linear modulation. This condition corresponds to the maximum speed (33), where $\bar{v}_S$ is orthogonal to the stator current $\bar{i}_S$ and the output power is zero.

III. CONTROL SCHEME

The control scheme shown in Fig. 5 can be divided into two parts. The first part concerns the control of the inverter A, which is connected to the power supply. It includes the control loops for speed, flux, and stator currents. The aim of the second part is to control the dc voltage of the floating bridge and to compensate the reactive power of the motor.

A. Control of Flux, Speed, and Stator Currents

PI regulators (a) and (b) control the d–q components of the stator currents. Feed-forward signals are added to the output of these regulators to compensate the back electromotive force of the motor and the voltage generated by inverter B. To reduce the effect of a mismatch in the machine parameters, a closed-loop flux weakening strategy is used to regulate the stator flux. PI regulator (c) defines the reference value of current i_{Sd} by

comparing the voltage request of inverter A with $V_{A,\max}$. If it is greater, the control system reduces $i_{Sd,\text{ref}}$ and decreases the stator flux. Finally, controller (d) chooses the reference value $i_{Sq,\text{ref}}$ on the basis of the speed error. This value is bounded by the value $\sqrt{I_{\max}^2 - i_{Sd,\text{ref}}^2}$ in order to satisfy the current constraint in every operating condition.

B. Control of the Floating Capacitor and of the Reactive Power

Regulator (e) keeps the dc-link voltage E_B at the reference voltage $E_{B,\text{ref}}$, whose level is adjusted depending on the voltage resulting from (16), which is necessary to compensate the reactive power of inverter A. Although the dc-link voltage of the floating capacitor bridge is variable during the speed transient, the control equation is approximately linear. In fact, (7) can be rewritten as follows:

$$\frac{d}{dt}\left(\frac{1}{2}CE_B^2\right) = P_B \tag{36}$$

where the active power P_B of inverter B is

$$P_B = K_E\left(E_{B,\text{ref}}^2 - E_B^2\right). \tag{37}$$

Combining (36) and (37), one finds a first-order differential equation of E_B^2

$$\tau\frac{d}{dt}E_B^2 + E_B^2 = E_{B,\text{ref}}^2 \tag{38}$$

where τ is a time constant equal to

$$\tau = \frac{C}{2K_E} \tag{39}$$

and K_E is the proportional grain of controller (e). To tune K_E, it can be noted that the reference value for $E_{B,\text{ref}}$ is roughly $\sqrt{3}$ times the optimal voltage $v_{B,\text{opt}}^q$ that allows maintaining the power factor of inverter A equal to 1. A coefficient K_m greater than one is used to consider that the transient term in (14) can require a significant voltage margin

$$E_{B,\text{ref}} = \sqrt{3}K_m\left|\frac{\omega\bar{\varphi}_S \cdot \bar{i}_S}{|\bar{i}_S|}\right|. \tag{40}$$

Equation (40) reveals that the dc-link voltage of inverter B is proportional to the motor speed. Therefore, to provide an accurate tracking of $E_{B,\text{ref}}$, the value of τ has to be chosen much smaller than the duration of the mechanical transients, which depend on the total inertia.

Since v_B^q is proportional to the motor speed, E_B tends to zero if the speed decreases, thus reducing the switching losses of inverter B. It is worth noting that, if the current i_{Sd} is kept equal to zero, it is not possible to pre-charge the floating capacitor until the torque is zero. In SPMSMs, in no-load conditions, the stator current does not circulate, and the active and reactive powers exchanged by inverter B are both zero. The compensation of the reactive power Q_A is achieved with PI (f). The feed-forward signal v_B^q given by (13) is added to the output of PI (f) to improve the dynamic performance.

Both PI regulators (e) and (f) are implemented in the reference frame aligned with the stator current space vector.
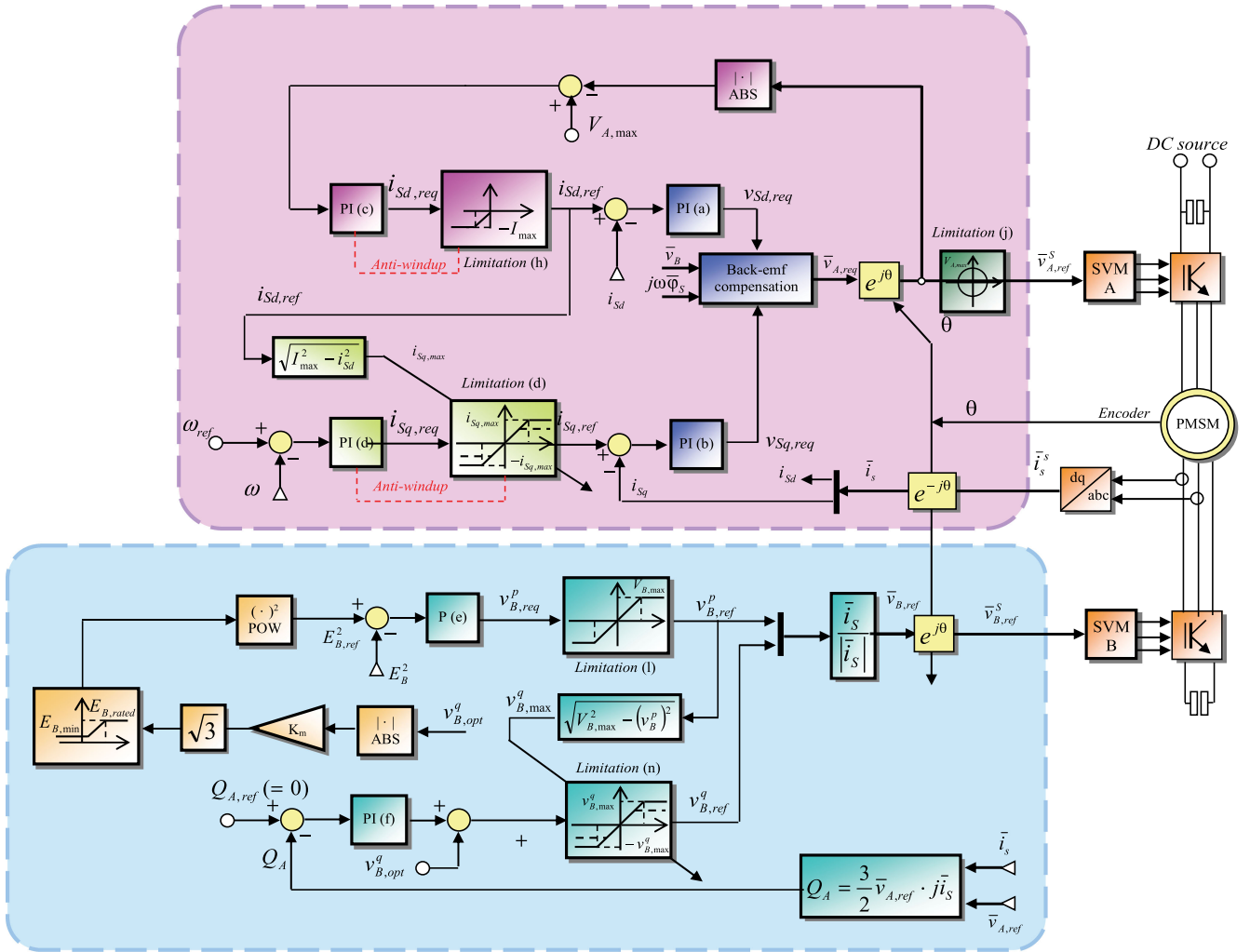
Fig. 5. Block diagram of the control scheme for the open-end winding permanent magnet machine fed by the dual-inverter system.
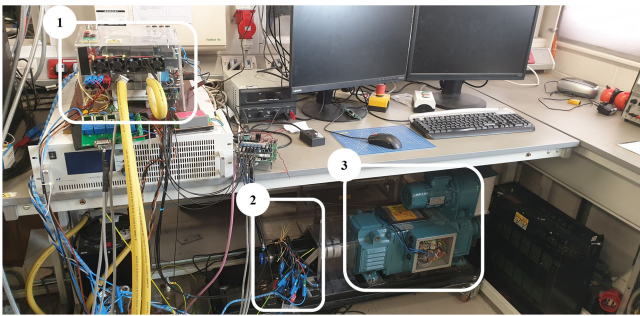

Fig. 6. Picture of the test bench, consisting of the measuring equipment and the dual inverter (1), the open-end winding brushless motor (2), and an electric machine (3) operating as a load.

IV. EXPERIMENTAL RESULTS

Experimental tests have been carried out by means of a small laboratory prototype to verify the feasibility of the developed control scheme. The picture of the test bench is shown in Fig. 6. It depicts the test bench, consisting of the measuring instruments and the dual inverter (1), which feeds the open-end

winding brushless motor (2) coupled with an electric machine (3) acting as a load. Inverter A is based on an insulated gate bipolar transistor (IGBT) power module (FF400R12KT3IGBT) developed by Infineon, whereas inverter B is based on an SiC power module (BSM180D12P2C101) by Rohm. The switching frequency is 8 kHz. The commutation dead-time of inverter A is 2 μs, while the commutation dead-time of inverter B is 1 μs. The control board is the uCube system designed at the University of Nottingham [17]. The parameters of the drive are the same shown in Table I. The measured signals have been acquired, transferred to a PC and plotted with Matlab.

Fig. 7 compares the behavior of a single inverter drive with the dual inverter drive during a start-up transient. If the rotor speed is below the base speed, current i_{Sd} is zero and the current i_{Sq} is equal to the maximum value $I_{\max}$ to generate the maximum torque. The phase angle Φ between the current vector and voltage vector is roughly constant with speed and can be calculated as follows:

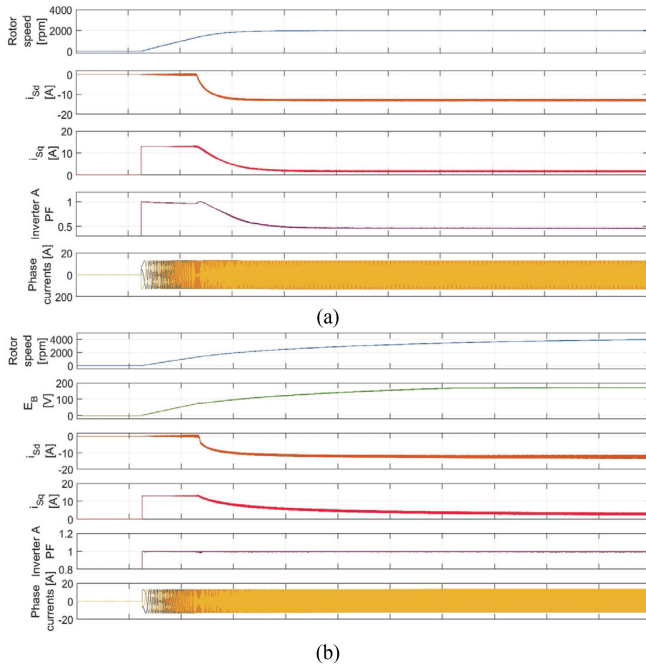$$\tan \Phi = \frac{L_S I_{\max}}{\varphi_e}. \tag{41}$$

Fig. 7. Experimental behavior of the SPMSM drive during a speed transient from zero to the maximum speed in case of (a) single inverter and (b) dual inverter. Time scale: 1 s/div.
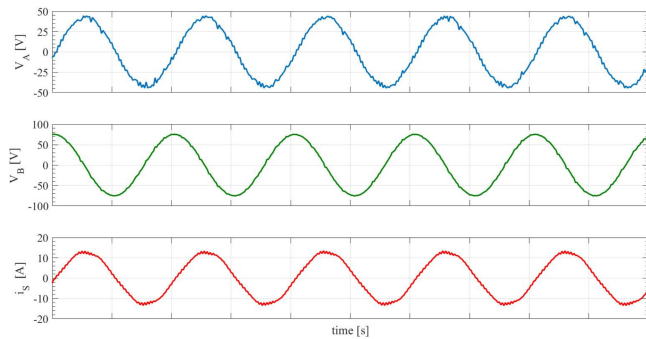

Fig. 8. Steady-state behavior of the dual inverter system. Waveforms of the reference voltage of inverters A and B (d-component in the stationary reference frame), and motor phase current at the mechanical speed of $2.5\omega_{base}$ (5 ms/div).

Fig. 9 Performance of the drive fed by the dual inverter (red) and the single inverter (blue) systems.

In the flux weakening region, the power factor of a single inverter drive rapidly decreases along with the q component of the stator current, thus limiting the overall performance.

Conversely, Fig. 7(b) shows that the compensation of the reactive power of inverter A allows producing higher torque values at high speed. Fig. 7(b) shows that, if the rotor speed is twice the maximum speed achievable by the same motor fed by a single inverter system, the power factor of inverter A is unity. This means that the drive still operates in the constant power speed range, below the value of the rotor speed given by (31).

Fig. 8 shows the waveforms of the d-component of the reference voltage vectors of inverters A and B, in the stationary reference frame, and the phase current of the machine at a mechanical speed of $2.5\omega_{base}$ (4000 r/min) for the dual inverter
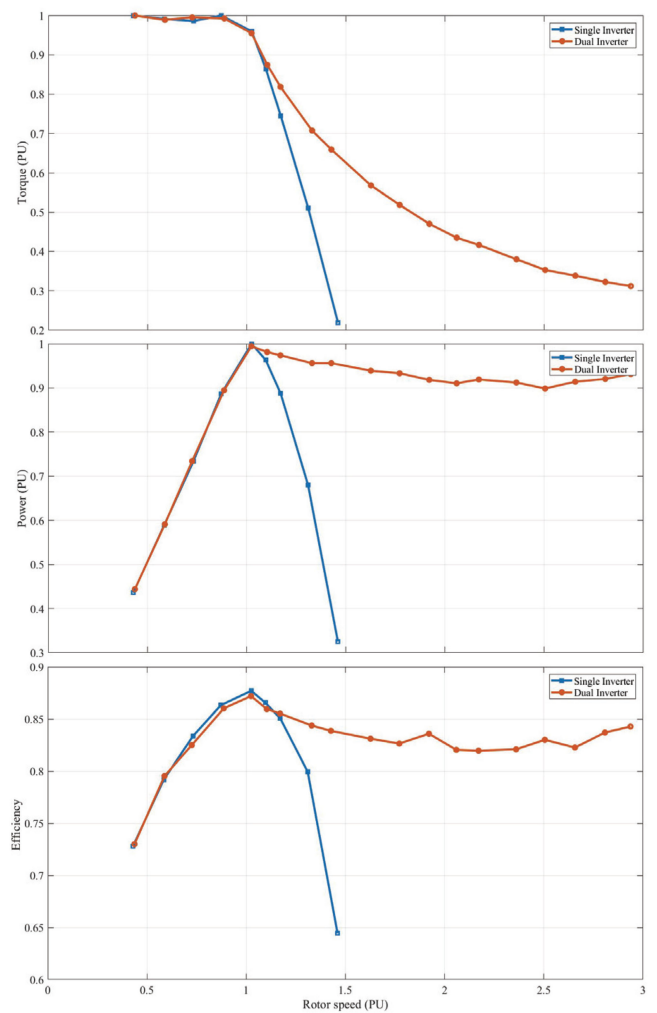
system. As can be seen, the stator current is reasonably sinusoidal, and it is in phase with the reference voltage of inverter A, as expected for a unity power factor. Similarly, the waveform of the reference voltage of inverter B is sinusoidal, but it leads the voltage waveform of inverter B by 90°.

The primary purpose of the developed drive is to extend the speed range of the drive and not to improve the drive efficiency. However, the analysis of the losses is essential to assess the drive performance. Fig. 9 compares the trend of the mechanical torque, the output power, and the efficiency of the drive when the machine is fed by a single inverter and the dual inverter system, and the ratio $E_{B,max}/E_{A,max}$ is equal to 2. The efficiency was measured as the ratio of the output mechanical power and the input electrical power. The input voltage, filtered by a bank of capacitors, was generated by a LAB-HP-E 15600 high power dc source, which can provide up to 15 kW at 600 V and 25 A. Since the input voltage was constant, the current ripple did not affect the average value of the input power, which could be measured with reasonable accuracy, around 1%. The mechanical power was estimated with similar accuracy as the product of the mechanical torque and speed.

Fig. 8 shows that the efficiency of the single-inverter system is slightly higher than that of the dual-inverter system at low speed. This fact merits some comments. In the low-speed range, under the same conditions of speed, torque level, and dc-link voltage, the dual-inverter drive may generate more losses than the single inverter drive, due to the switching and conduction losses of the floating capacitor bridge. It is difficult to evaluate the losses of inverter B because they are a function of the stator currents and the variable dc-link voltage, which is optimized by the control system depending on the operating conditions.

However, since inverter B operates as a power factor corrector, the mechanical power generated by the dual-inverter system in the low-speed range can be slightly higher than that produced by the single-inverter system. Equation (26) shows that the base speed of a single-inverter drive is lower than that of a dual inverter drive and proportional to the input power factor at the base speed. Consequently, if the iron losses are neglected, the input power of the dual-inverter system is P_A, the output power of the single-inverter system is $P_A \cos\Phi_{\text{base}}$, with a difference equal to $P_A(1 - \cos \Phi_{\text{base}})$.

One can conclude that, despite the higher losses, the overall efficiency of the dual-inverter drive in the low-speed range may be higher or lower than the efficiency of the single-inverter drive, depending on whether the increase in the output power counterbalances the additional inverter losses or not.

Some simulation results carried out with PLECS showed that, in rated conditions, the total power losses of inverter A and B are respectively about 20 and 10 W. The stator Joule losses of the motor are about 60 W. Hence, the presence of inverter B increases the drive losses by 12%.

In contrast, the theoretical value of $\cos\Phi_{\text{base}}$ for the laboratory prototype is 0.986, which makes the power improvement negligible (about 12 W) and justifies the slightly lower efficiency of the dual-inverter drive compared to the single-inverter drive.

However, the dual inverter system allows obtaining a threefold increase in the maximum speed of the machine. The output power decreases only by 10% up to 3 times the base speed. In the flux weakening region, while the power factor of the single inverter drive rapidly decreases and its active power drops to zero, the power factor of the dual inverter drive remains constant. In these operating conditions, the comparison between the single and dual inverter drives cannot be performed because this speed range is far beyond the maximum speed that the drive can reach when fed by a single inverter.

V. Conclusion

A dual PWM inverter system feeding an open-end winding SPMSM offers significant advantages in high-speed applications. The floating bridge inverter acts as a power factor compensator, allowing the primary inverter to operate at unity power factor and to exploit the available power source to generate active power only. The improvement in the resultant drive consists in a significant extension of the constant power speed range compared to the single-inverter application (up to three in the experimental tests). Furthermore, the control of

the floating bridge voltage, according to the operating conditions, allows reducing the switching losses of the second inverter.

Below the base speed, the power factor of the main inverter can be unity, above the base speed, the constant speed range can be extended up to a speed value given by (29), which is related to the dc-link voltage the floating inverter. Finally, a further speed extension is possible, although the power factor of the main inverter cannot be unity any more.

References

[1] A. M. El-Refaie and T. M. Jahns, "Comparison of synchronous PM machine types for wide constant-power speed operation: Converter performance," *IET Elect. Power Appl.*, vol. 1, pp. 217–222, 2007.

[2] B. Wang et al., "Overall assessments of dual inverter open winding drives," in *Proc. IEEE Int. Elect. Mach. Drives Conf.*, May 2015, pp. 1029–1035.

[3] B. A. Welchko and J. M. Nagashima, "The influence of topology selection on the design of EV/HEV propulsion systems," *IEEE Power Electron. Lett.*, vol. 1, no. 2, pp. 36–40, Jun. 2003.

[4] L. Rovere, A. Formentini, G. L. Calzo, P. Zanchetta, and T. Cox, "IGBT-SiC dual fed open end winding PMSM drive," in *Proc. IEEE Int. Elect. Mach. Drives Conf.*, May 2017, pp. 1–7.

[5] L. Rovere, A. Formentini, G. L. Calzo, P. Zanchetta, and T. Cox, "Zero-sequence voltage elimination for dual fed common dc-link open-end winding PMSM high speed starter-generator, Part I: Modulation," *IEEE Trans. Ind. Appl.*, vol. 55, no. 6, pp. 7804–7812, Nov./Dec. 2019.

[6] L. Rovere, A. Formentini, G. L. Calzo, P. Zanchetta, and T. Cox, "Zero-Sequence voltage elimination for dual fed common dc-link open-end winding PMSM high speed starter-generator, Part II: Dead time hysteresis control of zero sequence current," *IEEE Trans. Ind. Appl.*, vol. 55, no. 6, pp. 7813–7821, Nov./Dec. 2019.

[7] J. S. Park and K. Nam, "Dual inverter strategy for high operation of HEV permanent magnet synchronous motor," in *Proc. Ind. Appl. Conf.*, 2006, pp. 488–494.

[8] T. Gerrits, C. G. E. Wijnands, J. J. H. Paulides, and J. L. Duarte, "Dual voltage source inverter topology extending machine operating range," in *Proc. IEEE Energy Convers. Congr. Expo.*, 2012, pp. 2840–2846.

[9] Y. Lee and J.-I. Ha, "Power enhancement of dual inverter for open-end permanent magnet synchronous motor," in *Proc. Appl. Power Electron. Conf. Expo.*, 2013, pp. 1545–1551.

[10] R. U. Haque, M. S. Toulabi, A. M. Knight, and J. Salmon, "Wide speed range operation of PMSM using an open winding and a dual inverter drive with a floating bridge," in *Proc. IEEE Energy Convers. Congr. Expo.*, 2013, pp. 3584–3791.

[11] R. U. Haque, A. Kowal, J. Ewanchuk, A. Knight, and J. Salmon, "PWM control of a dual inverter drive using an open-ended winding induction motor," in *Proc. Appl. Power Electron. Conf. Expo.*, 2013, pp. 150–156.

[12] M. Mengoni, A. Amerise, L. Zarri, A. Tani, G. Serra, and D. Casadei, "Control scheme for open-ended induction motor drives with a floating capacitor bridge over a wide speed range," *IEEE Trans. Ind. Appl.*, vol. 53, no. 5, pp. 4504–4514, Sep./Oct. 2017.

[13] D. Pan, F. Liang, Y. Wang, and T. A. Lipo, "Extension of the operating region of an IPM motor utilizing series compensation," *IEEE Trans. Ind. Appl.*, vol. 50, no. 1, pp. 539–548, Jan./Feb. 2014.

[14] S. Chowdhury, P. Wheeler, C. Gerada, and S. L. Arevalo, "A dual inverter for an open end winding induction motor drive without an isolation transformer," in *Proc. IEEE Appl. Power Electron. Conf. Expo.*, Mar. 2015, pp. 283–289.

[15] A. Amerise, L. Rovere, A. Formentini, M. Mengoni, L. Zarri, and P. Zanchetta, "Control system for open-end winding surface PM synchronous machines with a floating capacitor bridge," in *Proc. IEEE Energy Convers. Congr. Expo.*, Sep. 2018, pp. 6585–6591.

[16] M. Pulvirenti, G. Scarcella, G. Scelba, and A. Testa, "On-line stator resistance and permanent magnet flux linkage identification on open-end winding PMSM drives," in *Proc. IEEE Energy Convers. Congr. Expo.*, Oct. 2017, pp. 5869–5876.

[17] A. Galassini, G. L. Calzo, A. Formentini, C. Gerada, P. Zanchetta, and A. Costabeber, "uCube: Control platform for power electronics," in *Proc. IEEE Workshop Elect. Mach. Design, Control Diagnosis*, 2017, pp. 216–221.

Albino Amerise received the M.Sc. (Hons.) and Ph.D. degrees in electrical engineering from the University of Bologna, Bologna, Italy, in 2015 and 2018, respectively.

In 2019, he was a Research Assistant with the Department of Electrical, Electronic and Information Engineering, "G. Marconi," University of Bologna. Since 2020, he has been with Magneti Marelli SpA, Corbetta, Italy. His research interests include vector control of induction machines and grid-connected converters.

Luca Rovere (Member, IEEE) received the M.S. (Hons.) degree in electrical engineering from the University of Genova, Genova, Italy, in 2015, and the Ph.D. degree in electrical and electronic engineering from the University of Nottingham, Nottingham, U.K., in 2019.

Before graduating, he spent a period at the Power Electronics and Machine Control Group of the University of Nottingham working on predictive controllers and sensorless control techniques. He is currently working as a Research Fellow with the University of Nottingham. His research interests include electrical drives, open-end winding machines and the modeling, design, and optimization of power electronics converters.

Andrea Formentini (Member, IEEE) received the M.S. degree in computer engineering and the Ph.D. degree in electrical engineering from the University of Genova, Genova, Italy, in 2010 and 2014, respectively.

He then started working as a Research Fellow in the Power Electronics, Machines and Control Group, University of Nottingham, Nottingham, U.K. Since 2018, he has been an Assistant Professor with the University of Nottingham. His research interests include control of electrical machine drives, power converters, and microgrids.

Michele Mengoni (Member, IEEE) was born in Forlì, Italy. He received the M.Sc. and Ph.D. degrees in electrical engineering from the University of Bologna, Bologna, Italy, in 2006 and 2010, respectively.

He is currently a Senior Assistant Professor with the Department of Electrical, Electronic and Information Engineering, "G. Marconi," University of Bologna. His research interests include design, analysis, and control of three-phase electric machines, multiphase drives, and ac/ac matrix converters.

Luca Zarri (Senior Member, IEEE) received the M.Sc. and Ph.D. degrees in electrical engineering from the University of Bologna, Bologna, Italy, in 1998 and 2007, respectively.

He is currently an Associate Professor with the Department of Electrical, Electronic, and Information Engineering, "Guglielmo Marconi," University of Bologna. He has authored or coauthored more than 150 scientific papers. His research activity concerns the control of power converters and electric drives.

Dr. Zarri is a Senior Member of the IEEE Industry Applications, IEEE Power Electronics and IEEE Industrial Electronics Societies.

Pericle Zanchetta (Fellow, IEEE) received the M.Eng. degree in electronic engineering and the Ph.D. degree in electrical engineering from the Technical University of Bari, Bari, Italy, in 1993 and 1997, respectively.

In 1998, he became an Assistant Professor of Power Electronics with the Technical University of Bari. In 2001, he became a Lecturer in control of power electronics systems in the PEMC research group with the University of Nottingham, Nottingham, U.K., where he is currently a Professor in Control of Power Electronics systems. He is also a part time Professor with the University of Pavia, Pavia, Italy. He has published more than 350 peer reviewed papers, he is a past Chair of the IEEE-IAS Industrial Power Converter Committee IPCC (2016–2017), Transactions Review Chair for IPCC (2018–2021). He is also a Chair of the IEEE-IAS Industrial Power Conversion Systems Department IPCSD 2020–2021. His research interests include control and optimization of power converters and drives, matrix and multilevel converters.